Morphology Control Enables Efficient Ternary Organic Solar Cells

*Yuanpeng Xie, Fan Yang, Yuxiang Li, Mohammad Afsar Uddin, Pengqing Bi, Bingbing Fan, Yunhao Cai, Xiaotao Hao, Han Young Woo, Weiwei Li, Feng Liu, and Yanming Sun**

Y. Xie, B. Fan, Y. Cai, Prof. Y. Sun

School of Chemistry

Beihang University

Beijing 100191, China

E-mail: sunym@buaa.edu.cn

Y. Fan, Prof. W. Li

Beijing National Laboratory for Molecular Science

Key Laboratory of Organic Solids

Institute of Chemistry, Chinese Academy of Sciences

Beijing 100190, P. R. China

Y. Li, M. A. Uddin, Prof. H. Woo

Department of Chemistry
College of Science, Korea University
Seoul 136-713, Republic of Korea

Prof. F. Liu

School of Physics and Astronomy and Collaborative Innovation

Center of IFSA (CICIFSA)

Shanghai Jiao Tong University

Shanghai 200240, P. R. China

P. Bi, Prof. X. Hao

School of Physics State Key Laboratory of Crystal Materials

Shandong University

Jinan 250100, P. R. China

Abstract: Ternary organic solar cell is a promising alternative to the binary counterpart due to its potential in achieving high performance. Although a growing number of ternary organic

solar cells have been recently reported, less effort has been devoted to morphology control. In this work, we fabricated ternary organic solar cells using a wide-bandgap polymer PBT1-C as the donor, a crystalline fused-ring electron acceptor ITIC-2Cl, and an amorphous fullerene derivative ICBA as the acceptors. It was found that ICBA could disturb π-π interactions of the crystalline ITIC-2Cl molecules in ternary blends and then helps to form more uniform morphology. As a result, incorporation of 20% ICBA in the PBT1-C:ITIC-2Cl blend enabled efficient charge dissociation, negligible bimolecular recombination, and balanced charge carrier mobilities. An impressive power conversion efficiency (PCE) of 13.4%, with a high fill factor (FF) of 76.8%, was eventually achieved, which represents one of the highest PCEs reported so far for organic solar cells. The results manifest that the adoption of amorphous fullerene acceptor is an effective approach to optimizing the ternary blend morphology and thereby increases the solar cell performance.

The past two decades have witnessed a continuous improvement in the power conversion efficiency (PCE) of bulk heterojunction (BHJ) organic solar cells (OSCs). [1-5] Combined developments in material and device engineering mainly contributed to such rapid advances.[6-8] For instance, devices based on a number of novel non-fullerene acceptor (NFA) materials have been recently reported with PCEs exceeding 12%,[9-17] which outperformed the photovoltaic performance of fullerene-based OSCs. However, it should be realized that the optical absorption bands of organic semiconductors are usually narrow, which restricts the BHJ layer to harvest sunlight over a wide range. To circumvent this problem, ternary structure comprising three different materials with complementary absorptions has acted as an attractive means of broadening the active layer absorption and thereby increasing the photocurrent.[18-23] In addition to the enhanced absorption profile, a favorable energy level alignment at the ternary BHJ interface can be formed by introducing an appropriate third material and hence improves the open-circuit voltage (V_{oc}).[24, 25] Meanwhile, ternary still inherits the simplicity of the fabrication process of binary OSCs.

Earlier studies on ternary OSCs mainly focused on either two donors/one fullerene acceptor or one donor/two fullerene acceptors.[26-35] However, the intrinsic drawbacks of fullerenes, such as weak visible light absorption and limited energy level tunability, hinder the further improvement of device performance.[36-38] Recent developments in NFAs offer a

wider choice of acceptor materials for ternary devices.[4, 5] Consequently, much effort has been devoted to the study of NFA-based ternary OSCs.[21, 22] Different ternary blends containing one NFA paired with two donors or one donor/one fullerene derivative exhibited high PCEs over 12%.[39-45] In terms of ternary blend incorporating two NFAs, impressive progresses have been also obtained.[46-52] For example, we have recently reported that high-performance ternary OSCs can be fabricated with a twisted perylene diimide acceptor (SdiPBI-Se) and a fused-ring electron acceptor (ITIC-Th).[53] These two NFAs are miscible and formed a homogeneous mixed phase, resulting in superior device performance, which offers a new direction in device optimization. Very recently, a high PCE of ~12.2% has been reported for ternary device using IT-M and ITCN acceptors.[54] These results highlight bright future for NFAs's application in ternary solar cells.

Noticeably, morphology is crucially important for BHJ OSCs. A bicontinuous interpenetrating network morphology is required to ensure efficient exciton dissociation and charge carrier transport.[55, 56] Since ternary blend comprises three components, molecular interactions between different materials can cause more complex morphology than its binary blend. The addition of a third component into ternary blend may result in large-scale phase separation, which is unfavorable for charge transport. Therefore, morphology control in

ternary blend remains very difficult, which becomes one of the main challenges of ternary OSCs.

In this contribution, we demonstrate an efficient approach to controlling the ternary blend morphology. We first fabricated binary device using a halogenated NFA, ITIC-2Cl,[57] and a wide-bandgap polymer donor, PBT1-C.[58] We found that the crystalline ITIC-2Cl molecules could easily form granular aggregates in the blend. An amorphous fullerene derivative, indene-C_{60} bisadduct, ICBA,[59] was adopted as the third component to optimize the ternary blend morphology. Upon the addition of 20% ICBA into PBT1-C:ITIC-2Cl blend, the morphology was substantially improved as the ITIC-2Cl aggregates obviously decreased. The favorable morphology enables balanced charge carrier mobilities, and reduced bimolecular recombination that result in high fill factor (FF). Moreover, the introduction of ICBA to ternary blends leads to increased V_{oc} due to its higher lowest unoccupied molecular orbital (LUMO) energy level than that of ITIC-2Cl. These features combined with the complementary absorption of ICBA with PBT1-C and ITIC-2Cl, yielded a high PCE of 13.4% (~21% higher than PBT1-C:ITIC-2Cl binary device) and an excellent FF of 76.8%. This work demonstrated the importance of morphology control in ternary OSCs and higher performance can be achieved by selecting appropriate materials to yield ideal BHJ morphology.

Chemical structures of PBT1-C, ITIC-2Cl, and ICBA are shown in **Figure 1**a. The corresponding energy level diagrams are illustrated in **Figure 1**b. The highest energy occupied molecular orbital (HOMO) and LUMO energy levels of PBT1-C and ICBA are -5.43 eV, -5.80 eV, -3.36 eV, and -3.74 eV, respectively. The HOMO enegy level of ITIC-2Cl lies between PBT1-C, and ICBA, suggesting that cascade charge transfer cannot occur in such ternary blend. In addition, compared with ITIC-2Cl, ICBA exhibits relatively higher LUMO of -3.74 eV, which can result in larger V_{oc}. Normalized UV-vis absorption spectra of PBT1-C, ITIC-2Cl, and ICBA neat films are shown in **Figure 1**c. It can be seen that PBT1-C has complementary spectra with ITIC-2Cl. Binary blend composed of these two materials showed broad light absorption in the range of 400-850 nm. The main absorption of ICBA is located in ultraviolet region, which helps to further extend the absorption of binary films (**Figure 1**d).

Ternary OSCs were fabricated with an inverted device structure of ITO /ZnO/active layer/MoO_3/Ag. The current density-voltage (*J*-*V*) curves of OSCs fabricated with different ICBA contents are illustrated in **Figure 2**a and the detailed device parameters are summarized in **Table 1**. Binary devices based on PBT1-C:ITIC-2Cl and PBT1-C:ICBA blends were firstly fabricated. PBT1-C:ITIC-2Cl device exhibited a PCE of 11.1%, with a short-circuit current (J_{sc}) of 18.34 mA cm^{-2}, a FF of 70.7%, and a V_{oc} of 0.86 V. In contrast,

PBT1-C:ICBA device showed a much lower PCE of 2.2%, with lower J_{sc} (5.41 mA cm^{-2}) and FF (40.5%), but a higher V_{oc} (0.99 V). We further fabricated ternary devices to investigate the influence of ICBA contents on the photovoltaic performance. As shown in **Figure 2**a, incorporating 10% ICBA into PBT1-C:ITIC-2Cl blend significantly boosted PCE to 12.5% with a J_{sc} of 19.13 mA cm^{-2}, a V_{oc} of 0.87 *V* and a FF of 74.9%. Further increasing ICBA content to 20% continuously increased the solar cell performance. Correspondingly, the champion device exhibited an impressive PCE of 13.4%, with a J_{sc} of 19.58 mA cm^{-2}, a V_{oc} of 0.89 *V* and a high FF of 76.8%. To the best of our knowledge, the PCE of 13.4% is among the highest values reported so far for ternary solar cells (**Table S1** and **Figure 2**c). The device parameters except the V_{oc} were found to decrease as ICBA contents in ternary blends exceeded 30%. The PCE of the ternary blend with 90% ICBA is quite comparable to that of PBT1-C:ICBA. It is interesting to note that V_{oc} gradually increased with increasing ICBA contents in ternary blends. This behavior can be explained by the result of its high LUMO level, which contributed to such increased V_{oc}. External quantum efficiency (EQE) spectra were shown in Figure 2b. PBT1-C:ITIC-2Cl reference device exhibited a broad spectral range from 300 nm to 850 nm with a maximum EQE value of 78.24% at 670 nm. The addition of 20% ICBA led to entirely enhanced EQE spectra with a maximum value of 82.36% at 720 nm. The calculated J_{sc} from the EQE spectra is 18.88 mA cm^{-2}, agreeing well with the measured value (19.58 mA cm^{-2}).

To study charge recombination kinetics in binary and ternary devices, J_{sc} versus a function of light intensity (I) was measured (Figure S1a**)**. In general, a power law dependence between J_{sc} and I can be expressed as $J_{sc} \propto I^{\alpha}$,[60] where α is the power-law exponent. The α values are 0.95, 0.85, and 1.0 for OSCs based on PBT1-C:ITIC-2Cl, PBT1-C:ICBA, and PBT1-C:ICBA:ITIC-2Cl (1:0.2:0.8) blends, respectively, reflecting negligible bimolecular recombination in the ternary device. The V_{oc} versus light intensity of binary and ternary devices was shown in Figure S1b. The slopes of PBT1-C:ITIC-2Cl and PBT1-C:ICBA binary devices are 1.47 and 1.62 kT/q, respectively, while the slope of PBT1-C:ICBA:ITIC-2Cl (1:0.2:0.8) teranry device is 1.25 kT/q, indicating that the addition ICBA into the ternary blend reduced the trap-assisted recombination.[61]

Moreover, charge dissociation probability P(E,T) was calculated from photocurrent density (J_{ph}) versus effective voltage (V_{eff}) (Figure S1c). The P(E,T) values are 97.3%, 98.4%, and 85.3% for devices with 0%, 20% and 100% ICBA contents, respectively, indicating that the addition of ICBA into the ternary blends increased charge dissociation capability. The electron (μ_e) and hole (μ_h) mobilities of ternary blends were measured by space charge-limited current (SCLC) method (Figure S2 and Figure 2b). As shown in Figure 2b, the ICBA content in ternary blends has slight influence on the hole mobilities. On the contrary, the electron mobilities strongly correlated with the ICBA content, which dropped

rapidly from 8.9×10^{-4} cm^2 V^{-1} s^{-1} to 3.1×10^{-5} cm^2 $V^{-1}s^{-1}$ as the ICBA content increases from 0% to 100% in ternary blends. In particular, ternary devices with 20% ICBA shows hole and electron mobilities of 6.1×10^{-4} cm^2 V^{-1} s^{-1} and 5.7×10^{-4} cm^2 V^{-1} s^{-1}, respectively, with μ_h/μ_e value of 1.07. Reduced recombination, efficient charge dissociation, and the balanced charge transport afford a better understanding of the high J_{sc} and FF achieved in ternary devices.

Steady state photoluminescence (PL) and time-resolved photoluminescence (TRPL) studies have been performed to investigate the energy/charge transfer between PBT1-C, ITIC-2Cl, and ICBA. As illustrated in **Figure 3**, ITIC-2Cl neat film shows relatively weak emission intensity at 790 nm with fluorescence lifetime (τ) of 139 ps, while ICBA neat film presents strong PL intensity at 740 nm with longer fluorescence lifetime (τ = 893 ps). After blending ITIC-2Cl with ICBA, the PL spectrum of ICBA completely disappeared. On the contrary, the emission of ITIC-2Cl significantly increased, with fluorescence lifetime of 105 ps. It is also noted that the absorption spectrum of ITIC-2Cl strongly overlaps the emission of ICBA (Figure S3a). These results indicate the existence of efficient energy transfer from ICBA to ITIC-2Cl. Moreover, we also fabricated OSCs to determine the possibility of charge transfer between ITIC-2Cl and ICBA in ternary blends (Figure S3b). J_{sc} values of OSCs based on ITIC-2Cl and ICBA neat films are 0.23 mA cm^{-2}, and 0.04 mA cm^{-2}, respectively.

ITIC-2Cl:ICBA device showed a J_{sc} of 0.05 mA cm^{-2}, which is much lower than that of ITIC-2Cl-based device, revealing no charge transfer between ITIC-2Cl and ICBA.

PL quenching effect between the binary and ternary blends was further investigated. As displayed in Figure 3, PL of PBT1-C was mostly quenched by ITIC-2Cl. The addition of ICBA to PBT1-C:ITIC-2Cl blend can further quench the emission of PBT1-C. TRPL spectra of neat and blend films were measured by monitoring two emission wavelengths of 680 nm and 790 nm under 500 nm light excitation (**Figure 3**d). The lifetime of PBT1-C is 126 ps at 680 nm emission wavelength, and then decreased to 24 ps in the ternary film. Similarly, the lifetime of ITIC-2Cl is 139 ps at 790 nm emission wavelength and then decreased to 40 ps in the ternary film, suggesting efficient charge transfer in the blend.

Transmission electron microscopy (TEM) and atomic force microscopy (AFM) measurements were carried out to study the influence of ICBA on the active layer morphology (**Figure 4**a and Figure S4). As presented in **Figure 4**a, PBT1-C:ITIC-2Cl film showed a large number of aggregates in a length scale of a few tens of nanometers due to the crystalline nature of ITIC-2Cl molecules. The addition of 20% ICBA to PBT1-C:ITIC-2Cl obviously decreased the aggregation and improved the film morphology. The root-mean-square (RMS) roughness of the film decreased from 1.70 nm to 1.28 nm, agreeing well with the TEM results. Further increasing the ICBA contents lead to more uniform

fibrillar morphology. The results indicate that ICBA can influence the molecular packing and disturb the degree of aggregation of PBT1-C molecules, which is consistent well with the mobility trend observed in the ternary blend. In details, the hole mobility slightly increased and the electron mobility decreased in magnitude as ICBA contents increased in ternary blends.

Grazing-incidence wide-angle X-ray scattering (GIWAXS) was performed to probe molecular orientation and packing in both neat and blend films. **Figure 5** shows the 2D GIWAXS patterns and the corresponding out-of-plane and in-plane line cuts of films. The (100) reflections of PBT1-C, and ITIC-2Cl films were observed at q_{xy} = 0.26 and 0.33 Å^{-1}, corresponding to lamellar distances of 24.2 and 19.0 Å, respectively, and the (010) reflections were observed at q_z=1.65, 1.78 Å^{-1}, corresponding to π-π stacking distances of 3.8, 3.5 Å, respectively. Both PBT1-C, and ITIC-2Cl exhibited preferential face-on orientation as the π-π stacking peak mainly located in the out-of-plane direction. There are no obvious diffraction peaks for ICBA, indicative of its amorphous nature. When PBT1-C and ITIC-2Cl are blended, there presents strong (010) diffraction peak of ITIC-2Cl, demonstrating the dominant role of ITIC-2Cl on π-π stacking in blend films. The addition of 20% ICBA to PBT1-C:ITIC-2Cl blend led to a reduction of crystallinity of ITIC-2Cl, confirmed by the obviously decreased intensity of π-π stacking at 1.78 Å^{-1}. It was found that the ITIC-2Cl

diffraction features at 0.33 and 1.78 $Å^{-1}$ completely disappeared with ICBA content more than 30% in the blends, indicating that ICBA could form intimate mixing with ITIC-2Cl and thus reduces ITIC-2Cl molecular packing. Such an effect reduces electron mobility in ternary blends and thus leads to reduced device performance. The structure order of PBT1-C in BHJ blends remains quite robust, and not obvious reduction was seen when ICBA is introduced. Thus high quality nano fibrils can be maintained in these ternary blends, playing an important role to shape the BHJ morphology. Resonant soft x-ray scattering (RSoXS) was applied to study the phase separation of BHJ thin films and the results were shown in Figure S5. It is seen that in low ICBA concentration, a flat scattering curve was seen, which is due to the low contrast between PBT1-C and ITIC-2Cl. When ICBA is added, a broad scattering hump start to show up around 0.025 $Å^{-1}$ (25 nm phase separation). And PBT1-C:ICBA blend showed an obvious scattering hump around 0.015 $Å^{-1}$ (42 nm). Thus the addition of ICBA could form a new phase separated structure in ternary blends, making detailed analysis barely impossible. Correlation function fitting yielded the correlation length of 78, 178, 93, 50, 48 Å for ternary blends with 0%, 15%, 30%, 50%, 100% ICBA. And it is quite obvious that smaller sized phase separation does not yield best J_{sc} and PCE. This is due to the mismatch of electronic structure between PBT1-C and ICBA. As also observed in GIWAXS characterizations, the PBT1-C crystal fibrils can shape the BHJ morphology, the reduction of ITIC-2Cl upon more than 30% ICBA addition is detrimental to device performance. Thus the success of the

ternary blends with low ICBA addition should be in the framework of PBT1-C:ITIC-2Cl morphology framework. And the addition of ICBA into ITIC-2Cl could fine-tune the morphology, with the added benefit of improve V_{oc}, yielding high PCEs.

In summary, efficient ternary OSCs based on PBT1-C, ITIC-2Cl, and ICBA have been fabricated. ICBA has been employed as the third component in ternary blends because of its amorphous nature, which can disturb intermolecular π-π interactions of ITIC-2Cl and then influence the active layer morphology. As a result, a high PCE of 13.4% was achieved for the ternary blend with 20% ICBA, representing one of the best efficiencies reported in the literature so far for ternary OSCs. The efficient exciton dissociation, balanced charge mobility and negligible bimolecular recombination account for such high photovoltaic performance of ternary device. Our work provided a promising way to optimize the morphology of NFA-based ternary blends.

Acknowledgements

This work was financially supported by the National Natural Science Foundation of China (NSFC) (No. 21734001, 51473009, 21674007), and the International Science and Technology Cooperation Program of China (No. 2014DFA52820). HYW acknowledges the financial support from National Research Foundation (NRF) of Korea (2012M3A6A7055540, 2015M1A2A2057506). Portions of this research were carried out at beam lines 7.3.3 and 11.0.1.2 at the Advanced Light Source, which is supported by the Director, Office of Science, Office of Basic Energy Sciences, of the U.S. Department of Energy.

References

[1] Y. Liu, J. Zhao, Z. Li, C. Mu, W. Ma, H. Hu, K. Jiang, H. Lin, H. Ade, H. Yan, *Nat. Commun*. **2014**, *5*, 5293.

[2] W. Zhao, S. Li, H. Yao, S. Zhang, Y. Zhang, B. Yang, J. Hou, *J. Am. Chem. Soc*. **2017**, *139*, 7148.

[3] C. Sun, F. Pan, H. Bin, J. Zhang, L. Xue, B. Qiu, Z. Wei, Z.G. Zhang, Y. Li, *Nat. Commun*. **2018**, *9*, 743.

[4] P. Cheng, G. Li, X. Zhan, Y. Yang, *Nat. Photon*. **2018**, *12*, 131.

[5] J. Hou, O. Inganas, R.H. Friend, F. Gao, *Nat. Mater*. **2018**, *17*, 119.

[6] L. Dou, J. You, Z. Hong, Z. Xu, G. Li, R.A. Street, Y. Yang, *Adv. Mater*. **2013**, *25*, 6642.

[7] W. Li, L. Ye, S. Li, H. Yao, H. Ade, J. Hou, *Adv. Mater*. **2018**, 1707170.

[8] Y. Cai, L. Huo, Y. Sun, *Adv*. *Mater.* **2017**, *29*, 1605437.

[9] S. Li, L. Ye, W. Zhao, S. Zhang, S. Mukherjee, H. Ade, J. Hou, *Adv*. *Mater*. **2016**, *28*, 9423.

[10]Z. Fei, F.D. Eisner, X. Jiao, M. Azzouzi, J.A. Rohr, Y. Han, M. Shahid, A.S.R. Chesman, C.D. Easton, C.R. McNeill, T.D. Anthopoulos, J. Nelson, M. Heeney, *Adv*. *Mater*. **2018**, *30*, 1705209.

[11]B. Kan, J. Zhang, F. Liu, X. Wan, C. Li, X. Ke, Y. Wang, H. Feng, Y. Zhang, G. Long, R.H. Friend, A.A. Bakulin, Y. Chen, *Adv*. *Mater*. **2018**, *30*, 1704904.

[12]S. Li, L. Ye, W. Zhao, X. Liu, J. Zhu, H. Ade, J. Hou, *Adv*. *Mater*. **2017**, *29*, 1704051.

[13]X. Xu, T. Yu, Z. Bi, W. Ma, Y. Li, Q. Peng, *Adv*. *Mater*. **2018**, *30*, 1703973.

[14]Y. Cui, H. Yao, B. Gao, Y. Qin, S. Zhang, B. Yang, C. He, B. Xu, J. Hou, *J. Am*. *Chem*. *Soc*. **2017**, *139*, 7302.

[15]D. Sun, D. Meng, Y. Cai, B. Fan, Y. Li, W. Jiang, L. Huo, Y. Sun, Z. Wang, *J. Am*. *Chem*. *Soc.* **2015**, *137*, 11156.

[16]D. Meng, H. Fu, C. Xiao, X. Meng, T. Winands, W. Ma, W. Wei, B. Fan, L. Huo, N.L. Doltsinis, Y. Li, Y. Sun, Z. Wang, *J. Am. Chem. Soc.* **2016**, *138*, 10184.

[17]D. Meng, D. Sun, C. Zhong, T. Liu, B. Fan, L. Huo, Y. Li, W. Jiang, H. Choi, T. Kim, J.Y. Kim, Y. Sun, Z. Wang, A.J. Heeger, *J*. *Am*. *Chem*. *Soc.* **2016**, *138*, 375.

[18]L. Lu, M.A. Kelly, W. You, L. Yu, *Nat. Photon*. **2015**, *9*, 491.

[19]H. Li, K. Lu, Z. Wei, *Adv*. *Energy Mater*. **2017**, *7*, 1602540.

[20]N. Gasparini, X. Jiao, T. Heumueller, D. Baran, G.J. Matt, S. Fladischer, E. Spiecker, H. Ade, C.J. Brabec, T. Ameri, *Nat*. *Energy* **2016**, *1*, 16118.

[21]R. Yu, H. Yao, J. Hou, *Adv*. *Energy Mater*. **2018**, 1702814.

[22]H. Fu, Z. Wang, Y. Sun, *Solar RRL* **2017**, 1700158.

[23]N. Felekidis, E. Wang, M. Kemerink, *Energy Environ*. *Sci*. **2016**, 9, 257.

[24]P.P. Khlyabich, B. Burkhart, B.C. Thompson, *J*. *Am*. *Chem*. *Soc*. **2012**, *134*, 9074.

[25]L. Lu, W. Chen, T. Xu, L. Yu, *Nat*. *Commun*. **2015**, *6*, 7327.

[26]V. Gupta, V. Bharti, M. Kumar, S. Chand, A.J. Heeger, *Adv*. *Mater*. **2015**, *109*, 1789.

[27]Y. Yang, W. Chen, L. Dou, W.-H. Chang, H.-S. Duan, B. Bob, G. Li, Y. Yang, *Nat*. *Photon*. **2015**, *9*, 190.

[28]J.-S. Huang, T. Goh, X. Li, M.Y. Sfeir, E.A. Bielinski, S. Tomasulo, M.L. Lee, N. Hazari, A.D. Taylor, *Nat*. *Photon*. **2013**, *7*, 479.

[29]J. Zhang, Y. Zhang, J. Fang, K. Lu, Z. Wang, W. Ma, Z. Wei, *J*. *Am*. *Chem*. *Soc*. **2015**, *137*, 8176.

[30]T. Liu, L. Huo, X. Sun, B. Fan, Y. Cai, T. Kim, J.Y. Kim, H. Choi, Y. Sun, *Adv*. *Energy Mater*. **2016**, *6*, 1502109.

[31]G. Zhang, K. Zhang, Q. Yin, X.F. Jiang, Z. Wang, J. Xin, W. Ma, H. Yan, F. Huang, Y. Cao, *J. Am. Chem. Soc*. **2017**, *139*, 2387.

[32]T. Kumari, S.M. Lee, S.-H. Kang, S. Chen, C. Yang, *Energy Environ*. *Sci*. **2017**, *10*, 258.

[33]P. Cheng, Y. Li, X. Zhan, *Energy Environ*. *Sci*. **2014**, *7*, 2005.

[34]T. Ameri, T. Heumüller, J. Min, N. Li, G. Matt, U. Scherf, C.J. Brabec, *Energy Environ*. *Sci*. **2013**, *6*, 1796.

[35]Z. Li, X. Xu, W. Zhang, X. Meng, Z. Genene, W. Ma, W. Mammo, A. Yartsev, M.R. Andersson, R.A.J. Janssen, E. Wang, *Energy Environ*. *Sci*. **2017**, *10*, 2212.

[36]P. Cheng, C. Yan, Y. Wu, J. Wang, M. Qin, Q. An, J. Cao, L. Huo, F. Zhang, L. Ding, Y. Sun, W. Ma, X. Zhan, *Adv*. *Mater*. **2016**, *28*, 8021.

[37]A. Anctil, C.W. Babbitt, R.P. Raffaelle, B.J. Landi, *Environ. Sci. Technol.* **2011**, 45, 2353.

[38]J.E. Anthony, Chem. Mater. **2011**, *23*, 583.

[39]W. Zhao, S. Li, S. Zhang, X. Liu, J. Hou, *Adv. Mater.* **2017**, *29*, 1604059.

[40]X. Xu, Z. Bi, W. Ma, Z. Wang, W.C.H. Choy, W. Wu, G. Zhang, Y. Li, Q. Peng, *Adv. Mater.* **2017**, *29*, 1704271.

[41]K.H. Park, Y. An, S. Jung, H. Park, C. Yang, *Energy Environ. Sci.* **2016**, *9*, 3464.

[42]H. Lu, J. Zhang, J. Chen, Q. Liu, X. Gong, S. Feng, X. Xu, W. Ma, Z. Bo, *Adv. Mater.* **2016**, *28*, 9559.

[43]H. Yao, Y. Cui, R. Yu, B. Gao, H. Zhang, J. Hou, *Angew. Chem. Int. Ed.* **2017**, *56*, 3045.

[44]X. Ma, Y. Mi, F. Zhang, Q. An, M. Zhang, Z. Hu, X. Liu, J. Zhang, W. Tang, *Adv. Energy Mater.* **2018**, 1702854.

[45]H. Zhang, X. Wang, L. Yang, S. Zhang, Y. Zhang, C. He, W. Ma, J. Hou, *Adv. Mater.* **2017**, *29*, 1703777.

[46]D. Baran, R.S. Ashraf, D.A. Hanifi, M. Abdelsamie, N. Gasparini, J.A. Rohr, S. Holliday, A. Wadsworth, S. Lockett, M. Neophytou, C.J. Emmott, J. Nelson, C.J. Brabec, A. Amassian, A. Salleo, T. Kirchartz, J.R. Durrant, I. McCulloch, *Nat. Mater.* **2017**, *16*, 363.

[47]R. Yu, S. Zhang, H. Yao, B. Guo, S. Li, H. Zhang, M. Zhang, J. Hou, *Adv. Mater.* **2017**, *29*, 1700437.

[48]J. Zhang, C. Yan, W. Wang, Y. Xiao, X. Lu, S. Barlow, T.C. Parker, X. Zhan, S.R. Marder, *Chem. Mater.* **2018**, *30*, 309.

[49]P. Cheng, M. Zhang, T.K. Lau, Y. Wu, B. Jia, J. Wang, C. Yan, M. Qin, X. Lu, X. Zhan, *Adv. Mater.* **2017**, *29*, 1605216.

[50]T. Liu, X. Xue, L. Huo, X. Sun, Q. An, F. Zhang, T.P. Russell, F. Liu, Y. Sun, *Chem. Mater.* **2017**, *29*, 2914.

[51]M. Zhang, W. Gao, F. Zhang, Y. Mi, W. Wang, Q. An, J. Wang, X. Ma, J. Miao, Z. Hu, X. Liu, J. Zhang, C. Yang, *Energy Environ. Sci.* **2018**, *11*, 841.

[52]B. Kan, Y.-Q.-Q. Yi, X. Wan, H. Feng, X. Ke, Y. Wang, C. Li, Y. Chen, *Adv*. *Energy Mater*. **2018**, 1800424.

[53]T. Liu, Y. Guo, Y. Yi, L. Huo, X. Xue, X. Sun, H. Fu, W. Xiong, D. Meng, Z. Wang, F. Liu, T.P. Russell, Y. Sun, *Adv. Mater.* **2016**, *28*, 10008.

[54]W. Jiang, R. Yu, Z. Liu, R. Peng, D. Mi, L. Hong, Q. Wei, J. Hou, Y. Kuang, Z. Ge, *Adv. Mater.* **2018**, *30*, 1703005.

[55]A.J. Moulé, K. Meerholz, *Adv. Funct. Mater.* **2009**, *19*, 3028.

[56]F. Zhao, C. Wang, X. Zhan, *Adv*. *Energy Mater*. **2018**, 1703147.

[57]F. Yang, C. Li, W. Lai, A. Zhang, H. Huang, W. Li, *Mater. Chem. Front.* **2017**, *1*, 1389.

[58]T. Liu, L. Huo, S. Chandrabose, K.Chen, G. Han, F. Qi, X. Meng, D. Xie, W. Ma, Y. Yi, J. M. Hodgkiss, F. Liu, J.Wang, C. Yang, Y. Sun, *Adv. Mater.* **2018**, *30*, 1707353.

[59]Y. He, H.-Y. Chen, J. Hou, Y. Li, *J. Am. Chem. Soc.* **2010**, *132*, 1377.

[60]P. Schilinsky, C. Waldauf, C.J. Brabec, *Appl*. *Phys*. *Lett*. **2002**, *81*, 3885.

[61] M. Lenes, S. W. Shelton, A. B. Sieval, D. F. Kronholm, J. C. Hummelen, P. W. M. Blom *Adv. Funct. Mater.* **2009**, *19*, 3002.

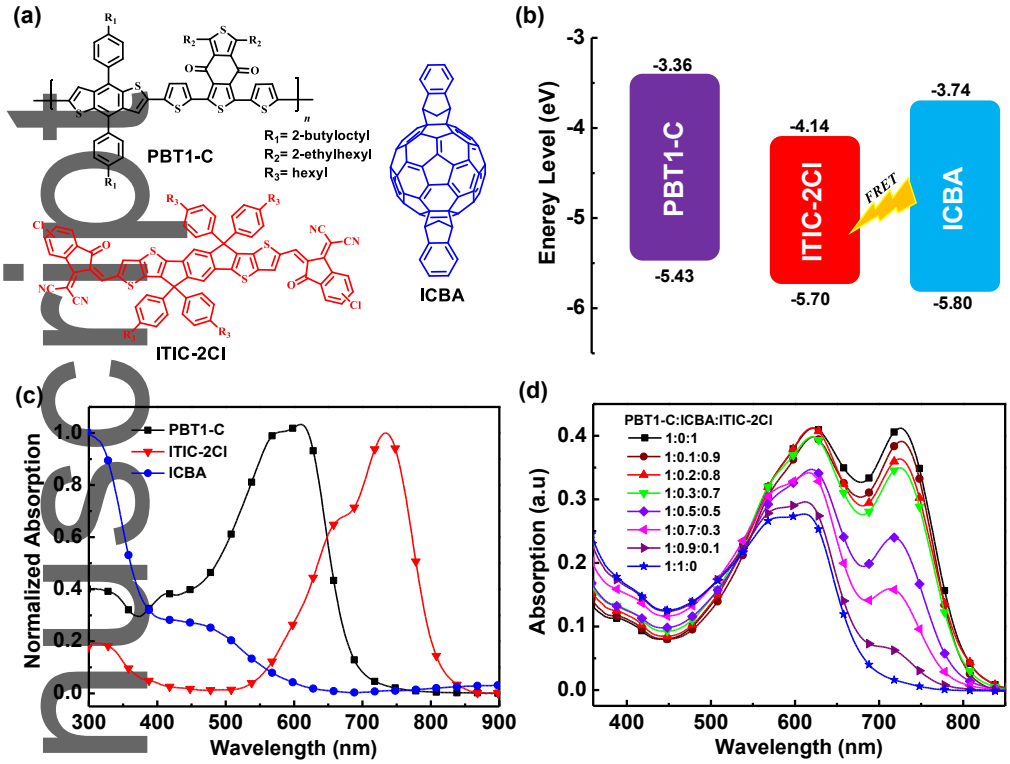

Figure 1. (a) Chemical structures of PBT1-C, ITIC-2Cl, and ICBA. (b) Energy levels of PBT1-C, ITIC-2Cl, and ICBA. (c) Normalized UV-vis absorption spectra of PBT1-C, ITIC-2Cl, and ICBA neat films. (d) UV-vis absorption spectra of ternary blends with different ICBA contents.

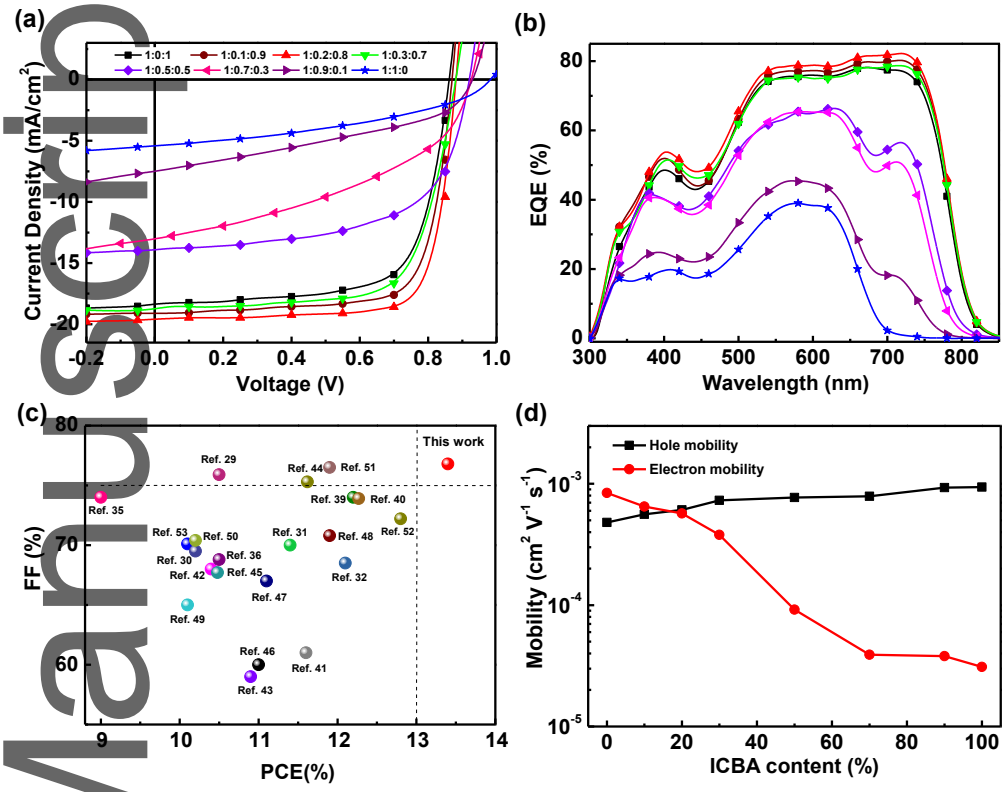

Figure 2. (a) Current-voltage (*J-V*) curves of ternary devices with different ICBA contents and (b) the corresponding EQE spectra of ternary devices. (c) Comparison of our results with representative PCE and FF values reported in the literature for ternary OSCs. (d) The hole and electron mobilities of ternary blends with different ICBA contents.

Table 1 Summary of device parameters of ternary organic solar cells with different ICBA contents.

PBT1-C:ICBA: ITIC-2Cl	J_{sc} (mA cm^{-2})	V_{oc} (V)	FF (%)	PCE[a] (%)	PCE_{max} (%)
1:0:1	18.03±0.40	0.86±0.02	70.3±2.1	10.9±0.2	11.1
1:0.1:0.9	18.90±0.32	0.87±0.03	74.1±1.1	12.2±0.3	12.5
1:0.2:0.8	19.30±0.39	0.89±0.02	75.9±1.2	13.0±0.4	13.4
1:0.3:0.7	18.54±0.51	0.89±0.04	73.5±1.5	12.1±0.4	12.5
1:0.5:0.5	13.80±0.30	0.92±0.03	60.0±1.0	7.6±0.2	7.8
1:0.7:0.3	12.98±0.30	0.93±0.01	39.5±1.3	4.8±0.1	4.9
1:0.9:0.1	7.40±0.30	0.93±0.02	38.6±0.9	2.7±0.1	2.8
1:1:0	5.40±0.20	0.98±0.03	38.7±0.3	2.1±0.1	2.2

a) The values are average PCEs from 10 devices

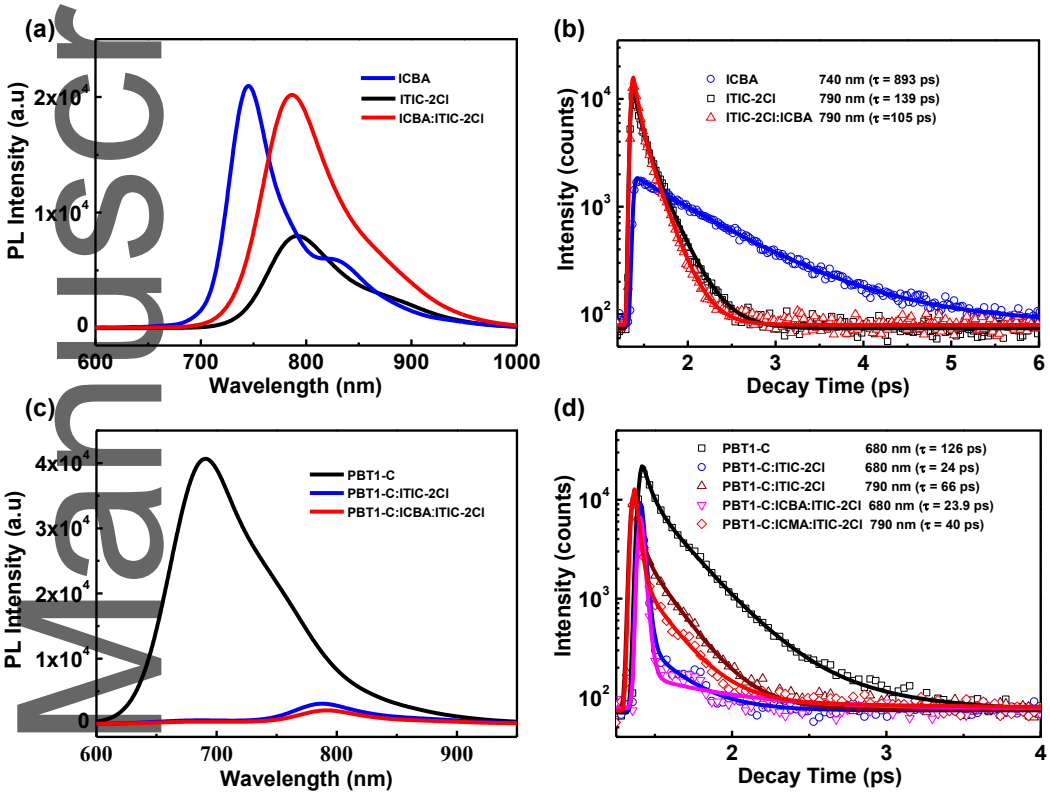

Figure 3. (a) PL and (b) TRPL spectra of ITIC-2Cl, ICBA, and ITIC:ICBA films. (c) PL spectra of PBT1-C, PBT1-C:ITIC-2Cl, and PBT1-C:ICBA:ITIC-2Cl (1:0.2:0.8) films. (d) TRPL spectra of PBT1-C, PBT1-C:ITIC-2Cl, and PBT1-C:ICBA:ITIC-2Cl (1:0.2:0.8) films (excited at 500 nm and monitored at 680 and 790 nm, respectively).

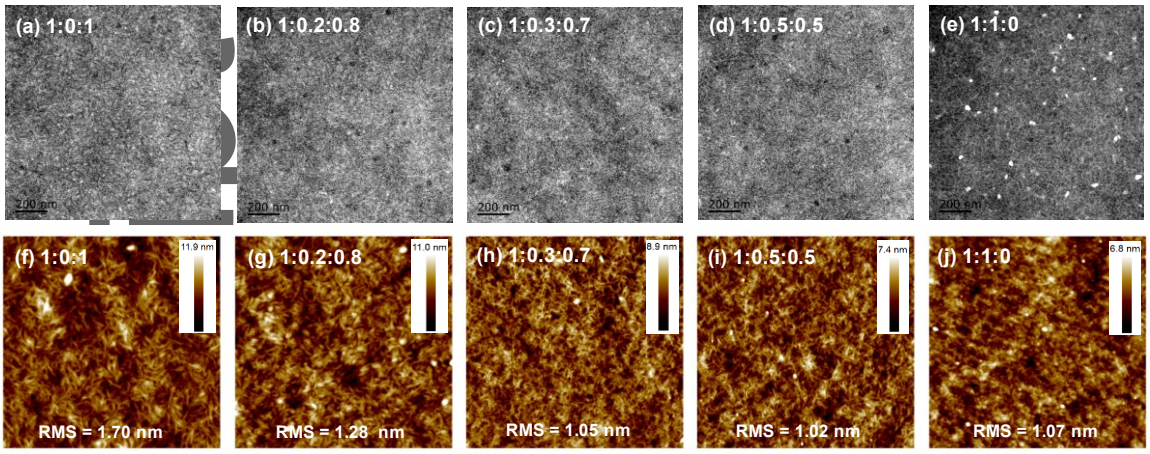

Figure 4. (a-e) TEM and (f-j) AFM height images of ternary blends with different ICBA contents.

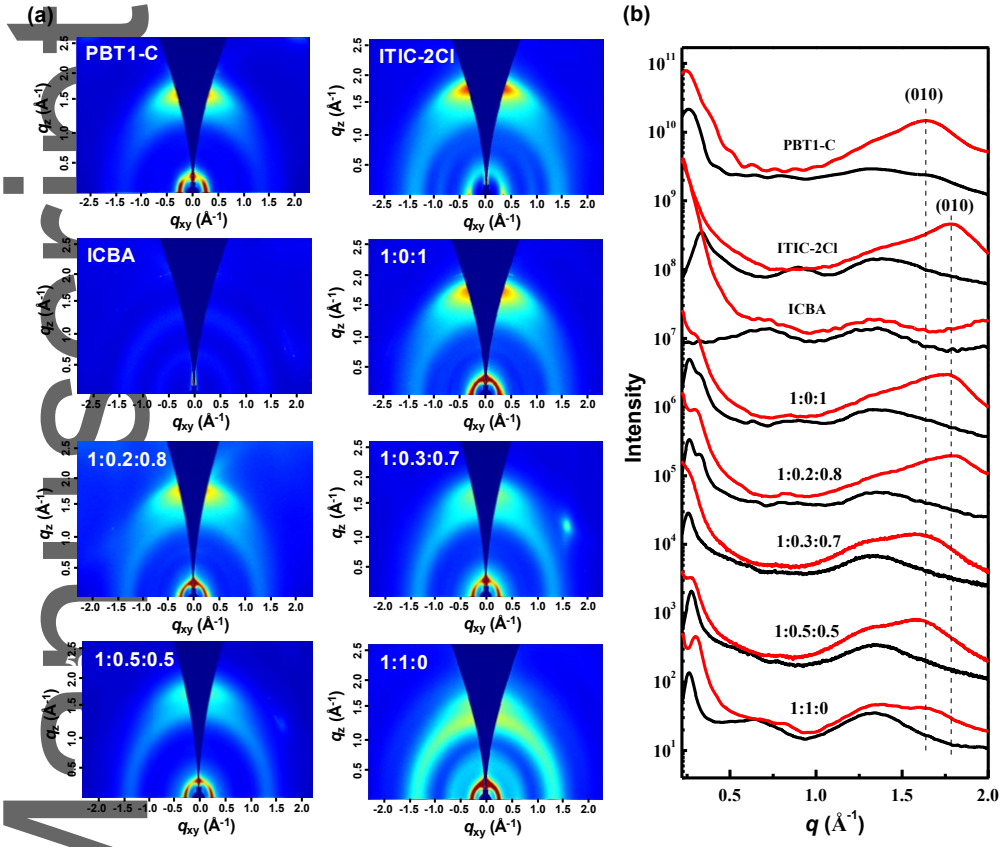

Figure 5. (a) 2D GIWAXS patterns and (b) the out-of-plane and in-plane line-cut profiles of PBT1-C, ITIC-2Cl, ternary blends with different ICBA contents.

Table of Contents

Ternary organic solar cells based on a polymer donor PBT1-C, a fullerene derivative ICBA, and a crystalline fused-ring electron acceptor ITIC-2Cl were fabricated. The addition of 20% ICBA to PBT1-C:ITIC-2Cl led to favorable morphology, which yielded an impressive efficiency of 13.4%, and a high fill factor of 76.8%, indicating that the use of amorphous fullerene acceptor is an effective way to optimize the ternary blend morphology.

Keywords: Organic solar cells, ternary structure, morphology, nonfullerene acceptor, ICBA

Yuanpeng Xie, Fan Yang, Yuxiang Li, Mohammad Afsar Uddi, Pengqing Bi, Bingbing Fan, Yunhao Cai, Xiaotao Hao, Han Young Woo, Weiwei Li, Feng Liu, and Yanming Sun*

Morphology Control Enables Efficient Ternary Organic Solar Cells

ToC figure

Author/s:
Xie, Y;Yang, F;Li, Y;Uddin, MA;Bi, P;Fan, B;Cai, Y;Hao, X;Woo, HY;Li, W;Liu, F;Sun, Y

Title:
Morphology Control Enables Efficient Ternary Organic Solar Cells

Date:
2018-09-20

Citation:
Xie, Y., Yang, F., Li, Y., Uddin, M. A., Bi, P., Fan, B., Cai, Y., Hao, X., Woo, H. Y., Li, W., Liu, F. & Sun, Y. (2018). Morphology Control Enables Efficient Ternary Organic Solar Cells. ADVANCED MATERIALS, 30 (38), https://doi.org/10.1002/adma.201803045.